Eur. J. Mech. A/Solids 18 (1999) 93–113

Numerical study of the critical impact velocity in shear

Janusz Roman Klepaczko *, Maciek Klósak

Laboratoire de Physique et Mécanique des Matériaux, CNRS – UMR 7554, ISGMP, Université de Metz, Ile du Saulcy, 57045 Metz cedex 01, France

(Received 24 July 1997; accepted 16 June 1998)

Abstract – The phenomenon of critical impact velocity (CIV) in shear is studied in this paper. Deformation trapping due to thermoplastic instability caused by the propagation of plastic waves are the main physical reasons for CIV in shear. A simple analytical approach is offered on how to estimate the value of CIV. A numerical study of impact shearing of a layer with a small geometric imperfection has been performed by the FE code ABAQUS, and available experimental results verified for VAR 4340 steel, ≈ 50 HRC, obtained by direct impact on modified double shear (MDS) specimen. In particular, the numerical study was focused on the effect of the imposed velocity on the spatial deformation of the layer. Seventeen velocities were assumed in FE calculations from quasi-static to 160 m/s. Two modes of shear deformation of the layer were found: in the first mode all plastic deformation concentrates in the middle of the layer, and in the second near the surface where the shear velocity is imposed. CIV could be defined as a transition between those two modes. It has been shown that impact velocities higher than CIV lead to a substantial reduction in the total energy of strain localization. Overall good correlation with experimental results and physical intuition has been satisfactorily achieved. © Elsevier, Paris

critical impact velocity / shear / MDS specimen / numerical study / plastic deformation

1. Preliminary remarks

Localization of plastic deformation in the form of shear bands is a very common failure mode in many materials. At high strain rates the conditions of deformation are nearly adiabatic, which means that a large part of the mechanical work of plastic deformation is converted very rapidly into heat. If the process of deformation is nonhomogeneous the local heating of the material may be quite substantial and, as a consequence, due to thermal softening, the plastic flow becomes unstable. Finally, this process of thermal coupling leads to localization of plastic deformation in the form of adiabatic shear bands (ASB), a very narrow layer of shear deformation. The direction of ASB is normally aligned with a local direction of maximum shear stress. ASB has been studied more thoroughly over the last decade and many publications have appeared regarding this; we do not, however intend to review these publications. An early review was made by Rogers (1974), and a more recent review by Bai and Dodd (1992). The majority of publications on ASB are based on a quasi-static approach, i.e. the inertia effects are neglected or inertia is introduced in steady states without elastic–plastic wave propagation.

Recent experiments on construction and low-alloy steels with the relatively new experimental technique of direct impact on modified double shear specimen (MDS) (Klepaczko, 1994c) have revealed the existence of the critical impact velocity in shear (CIV). At impact velocities in the order of 100 m/s, plastic deformation in the form of ASB is always localized near the impact end of the sheared part of the specimen. The superposition of the adiabatic shear banding and adiabatic plastic waves in shear is the main cause of such localization.

* Correspondence and reprints

The phenomenon of CIV in shear was first predicted theoretically (Litonski, 1975; personal communication) and later included in the fragmentation modeling by by Erlich et al. (1980). Simple analytic formulas for CIV in shear have been discussed by Klepaczko (1994a, 1995). They confirm the experimental results that for some steels, CIV is around 100 m/s.

A numerical study of one-dimensional shear wave propagation in the half-space of a nonlinear material was considered by Wu and Freund (1984). The surface of the half-space was subjected to a time-dependent but uniform on the surface tangential velocity. A simple material model was assumed with strain hardening, thermal softening and rate sensitivity of the flow stress. It was found from an analysis by simple waves and by numerical calculations that a well-defined band of intense shear deformation can develop adjacent to the surface. The representative profiles of particle velocity and strain were found near the surface for different strain rate sensitivities (linear and logarithmic). It was concluded that the band of intense shear deformation could be developed without any imperfection.

Numerical studies of adiabatic shear banding by a quasi-static approach are quite numerous and they will not be discussed here; however, only few numerical studies are focused on adiabatic instability and localization at a wide range of nominal strain rates with $\dot{\Gamma}_n$ defined as the imposed velocity V_i divided by the thickness of the layer h_s, $\dot{\Gamma}_n = V_i/h_s$, (Klepaczko, 1993, 1994b; Klepaczko et al., 1988, 1996). Although inertia was included in these numerical studies, the initial conditions regarding how the shear velocity V_i was imposed on a layer of thickness h_s were not specified. In addition, elasticity was neglected in the numerical calculations. It was found that the nominal strain of instability Γ_{nc} defined by the maximum of shear stress $\partial\tau/\partial\Gamma = 0$, slightly increased as a function of the nominal strain rate, and at high strain rates in the order of $\approx 10^5 \mathrm{s}^{-1}$, the value of Γ_{nc} was the highest (impact velocity $V_i \approx 100\,\mathrm{m/s}$). The nominal shear strain at the final localization of ASB, Γ_{nl}, increased much faster as a function of the nominal strain rate than $\dot{\Gamma}_{nc}$. The ratio of these two quantities increased up to $(\Gamma_{nl}/\Gamma_{nc}) \approx 5.0$ at $\dot{\Gamma}_n = 10^5 \mathrm{s}^{-1}$. It is clear that this approach, without a precise definition of how the velocity was imposed on the layer, does not permit a numerical analysis of CIV in shear.

In order to analyze the effect of more realistic initial conditions defined by velocity which is imposed on the finite layer, on the process of instability and localization, a more systematic study of CIV in shear for VAR 4340 steel has been performed by the FE method.

2. Simple analytical modeling of CIV in shear

Previous analyses, both analytical and numerical, have indicated that during fast shearing the work of plastic deformation is dissipated locally as heat, and when the deformation time is short enough the heating process leads to the instability of plastic flow and localization. This happens because in spite of the constant cross-section of the deformed geometry (specimen in shear or torsion), the adiabatic heating tends to reduce the flow stress. This is the fundamental difference between shear and tensile deformation. In the case of a dynamic tensile test the simple wave solution for the rate-independent plastic waves, the so-called Taylor-Kàrmàn–Rakhmatulin approach, enables us to calculate the Kàrmàn CIV in tension using the isothermal approach and the isothermal Considère condition of stability $(d\sigma/d\varepsilon) = \sigma$, where σ and ε are respectively true stress and true strain (Kàrmàn and Duvez, 1950). Introduction of adiabatic heating in tension provides a more exact approach (Klepaczko, 1968).

In order to analyze CIV in shear, the condition for stability $(d\tau/d\Gamma) = 0$ can again be used. This condition can be satisfied in shear exclusively when thermal heating leads to thermal softening. If only one adiabatic stress–strain curve $\tau_A = f_A(\Gamma)$ is assumed, under such conditions the tangent modulus becomes zero, $(d\tau/d\Gamma)_A = 0$, and in the limit the plastic strain propagates at zero speed. This notion permits a simple analysis of CIV in shear.

As a first step, the conditions of adiabatic instability in shear will be discussed. Assuming the existence of the only one isothermal and one adiabatic shear stress–strain relation in the form $\tau = f(\Gamma)$ and $\tau_A = f_A(\Gamma)$, the condition for stability during adiabatic shearing leads to the formula

$$\left(\frac{d\tau}{d\Gamma}\right)_A = 0 \tag{1}$$

A number of authors have used the stability criterion (1), for example Recht (1964), to find the instability strain Γ_c when condition (1) is satisfied. A review of different formulas for Γ_c for different forms of constitutive relations has been made by Dormeval (1987).

Here a more general discussion of criterion (1) is provided, following Klepaczko (1994a). Because many authors use constitutive relations in the multiplication form

$$\tau = f_1(T) f_2(\Gamma) f_3(\dot{\Gamma}) \tag{2}$$

where T is the absolute temperature, and the strain-rate and temperature history effects are neglected, the stability criterion will be derived using Eqs (1) and (2). After differentiation of (2) and introduction into (1), the following relation is obtained

$$\left(\frac{\partial\tau}{\partial\Gamma}\right)_{T,\dot{\Gamma}} + \left(\frac{\partial\tau}{\partial T}\right)_{\Gamma,\dot{\Gamma}} \frac{dT}{d\Gamma} + \left(\frac{\partial\tau}{\partial\dot{\Gamma}}\right)_{T,\Gamma} \frac{d\dot{\Gamma}}{d\Gamma} = 0 \tag{3}$$

Condition (3) can be satisfied only in very specific processes of plastic deformation; one of them is adiabatic deformation at constant strain rate. Thus condition (3) reduces to

$$\left(\frac{\partial\tau}{\partial\Gamma}\right)_{T,\dot{\Gamma}} + \left(\frac{\partial\tau}{\partial T}\right)\left(\frac{d\tau}{d\Gamma}\right)_{\text{adiabatic}} = 0, \quad \dot{\Gamma} = \text{const.} \tag{4}$$

Assuming constitutive relation (2) it follows from the principle of energy conservation that

$$\left(\frac{dT}{d\Gamma}\right)_A = \frac{[1 - \xi(T, \Gamma)]\, f_1(T) f_2(\Gamma) f_3(\dot{\Gamma})}{\rho(T) C_V(T)} \tag{5}$$

where $\xi(T, \Gamma)$ is a coefficient taking into account the stored energy in the material, $\rho(T)$ is the mass density and $C_V(T)$ is the specific heat at constant volume. In general, both ρ and C_V are functions of the absolute temperature T. If the explicit forms of the partial differentials derived after (2) along with (5) are introduced into (4), the condition (4) transforms into

$$\left(\frac{\partial f_2}{\partial\Gamma}\right) + f_2^2(\Gamma_c) f_3 \dot{\Gamma}\left(\frac{\partial f_1}{\partial T}\right)\frac{1 - \xi}{\rho C_V} = 0 \tag{6}$$

Since only $f_2(\Gamma_c)$ depends on the critical strain, the explicit relation for $f_2(\Gamma_c)$ is

$$f_2(\Gamma_c) = \left[-\frac{(\partial f_2/\partial\Gamma)}{(\partial f_1/\partial T\, f_3(\dot{\Gamma})(1 - \xi)}\right]^{1/2} \tag{7}$$

The expression $[\bullet]^{1/2}$ has real and imaginary parts. Inversion of $f_2(\Gamma_c)$ makes it possible to find Γ_c

$$\Gamma_c = f_2^{-1}[\bullet]^{1/2} \tag{8}$$

The existence of the real $f_2(\Gamma_c)$ is only possible if the expression $[\bullet]^{1/2}$ within the square brackets is positive. Since ρ, C_V and $(1 - \xi)$ must always be positive and the function of strain rate sensitivity, $f_3(\dot{\Gamma})$, is also assumed to be positive, the only term which may be negative is $(\partial f_2/\partial\Gamma)/(\partial f_1/\partial T)$. The most common case is the thermal softening which leads to a negative value of $(\partial f_1/\partial T)$, of course if $(\partial f_2/\partial\Gamma)$ is at the same time positive. The role of an increasing rate sensitivity is quite interesting, that is if $f_3(\dot{\Gamma})$ is an increasing

function of strain rate $\dot{\Gamma}$. A high rate sensitivity has a negative effect on the onset of adiabatic instability, that is Γ_c is reduced when strain rate is increased.

By analogy to CIV in tension, it is possible to construct a model of the plastic wave trapping in shear which is based on the criterion of adiabatic instability [Eqs (1) and (7)]. According to the rate-independent theory of elastic–plastic wave propagation, as applied to shear deformation, the wave equation is as follows

$$\frac{\partial^2 U}{\partial t^2} = C_{2p}(\Gamma)\frac{\partial^2 U}{\partial y^2} \tag{9}$$

where U is the displacement along the x-axis and wave propagation is along the y-axis (perpendicular).

The wave speed is defined as

$$C_{2p}(\Gamma) = \left(\frac{1}{\rho}\frac{d\tau}{d\Gamma}\right)^{1/2} \tag{10}$$

Equation (10) reduces to $C_2 = \sqrt{\mu/\rho}$ for the elastic case.

Along the characteristics $C_{2p} = \pm(dy/dt)$ the following relation holds

$$d\left[\int_0^{\Gamma_m} C_{2p}(\Gamma)d\Gamma - v\right] = 0 \tag{11}$$

where v is the mass velocity, $v = (\partial U/\partial t)$ and Γ_m is the wave amplitude. It is clear from (1), (4) and (10) that the wave-speed is zero if condition (1) is satisfied, that is $C_{2p}(\Gamma_c) = 0$, and at the same time the integral in (11) reaches the maximum value, thus

$$v_c = \int_0^{\Gamma_c} C_{2p}(\Gamma)_{\dot{\Gamma}} d\Gamma \tag{12}$$

where is Γ_c defined by Eq. (8). The wave speed in the adiabatic conditions of deformation at $\dot{\Gamma} = \text{const}$ can be written as

$$C_{2p} = \pm\left\{\frac{f_1 f_2 f_3}{\rho}\left[\frac{1}{f_2}\left(\frac{\partial f_2}{\partial \Gamma}\right) + f_2 f_3\left(\frac{\partial f_1}{\partial_T}\right)\frac{1-\xi}{\rho C_v}\right]\right\}^{1/2} \tag{13}$$

Finally, the critical impact velocity in shear is given by

$$v_c = \int_0^{\Gamma_c}\left\{\frac{f_1 f_2 f_3}{\rho}\left[\frac{1}{f_2}\left(\frac{\partial f_2}{\partial \Gamma}\right) + f_2 f_3\left(\frac{\partial f_1}{\partial T}\right)\frac{1-\xi}{\rho C_v}\right]\right\}^{1/2} d\Gamma \tag{14}$$

where the upper limit of integration is given by (8).

Explicit solutions for Γ_c, $C_{2p}(T)$ and v_c are possible if the constitutive relation is sufficiently simple.

Numerical evaluation of the set of equations (7), (8) and (14) for simple constitutive relations confirms that the order of CIV in shear is correct. For example, in the case of construction steel XC18 (AISI 1018) CIV was found at 98 m/s, a value very close to that of previous experimental findings (Klepaczko, 1993). The analysis which is given above permits an approximate evaluation of CIV in shear. The initial and boundary conditions cannot be precisely defined. It is clear that the FE method can provide a more precise analysis of this phenomenon.

3. Constitutive relation for VAR 4340 steel

It is well known that an adequate constitutive relation is the main condition for reliable FE results. A constitutive relation applied to the problems of plastic instability coupled with temperature must reflect properly the effect of strain hardening, temperature sensitivity and rate sensitivity at high strain rates on flow stress. The constitutive relation applied to the problem considered was specially developed to model experimental results

for VAR 4340 steel (Cowie, 1989; Klepaczko, 1993; Tanimura and Duffy, 1984) as well as some data for similar steels (Meyer and Staskewitsch, 1988).

After careful analyses of available experimental data for VAR 4340 steel of hardness ≈ 50 HRC the following general form was chosen

$$\tau = f_1(T)[f_2(T)f_3(\Gamma) + f_4(\dot{\Gamma}, T)] \tag{15}$$

where f_i are the functions of plastic shear strain Γ, shear strain rate $\dot{\Gamma}$ and absolute temperature T. Relation (15) is treated as a first approximation to the constitutive modeling. Further analyses of experimental data for steels have indicated that the strain hardening rate $\partial\tau/\partial\Gamma$ is temperature-dependent (e.g. Klepaczko, 1987a). The final general form of the constitutive relation used in majority of FE calculations is

$$\tau = f_1(T)[f_2(T)f_3(\Gamma, T) + f_4(\dot{\Gamma}, T)] \tag{16}$$

The explicit forms for Eqs (15) and (16) are assumed as follows

$$\tau = \frac{\mu(T)}{\mu_0}\left[B\left(\frac{T}{T_0}\right)^{-v}(\Gamma_0 + \Gamma_p)^n + \tau_0\left(1 - \frac{T}{D}\log\frac{\dot{\Gamma}_0}{\dot{\Gamma}}\right)^m\right] \tag{17}$$

where B, μ_0, v, n, m are respectively the modulus of plasticity, the shear modulus at $T = 300$ K, the temperature index, the strain hardening exponent and the logarithmic rate sensitivity; D, T_0, Γ_0 and $\dot{\Gamma}_0$ are normalization constants. The temperature dependence of the shear modulus is given by

$$\mu(T) = \mu_0\left(1 - AT^* - CT^{*2}\right), \quad T^* = T - T_{\min}, \quad T \geq T_{\min} \tag{18}$$

It should be noted that application of Eq. (17) is intended to be used at temperatures above a certain minimum temperature $T_{\min}$, in the present case $T_{\min} = 300$ K.

Relations (15) and (16) are distinguished by different forms of the strain hardening exponent n. In the first approach, i.e. Eq. (15), n was assumed as a constant throughout the FE analysis, whereas in the second approach i.e. Eq. (16), $n(T)$ is a linearly decreasing function of temperature

$$n(T) = n_0\left(1 - \frac{T}{T_m}\right) \tag{19}$$

where n_0 is the strain hardening exponent at $T = 0$ and T_m is the melting temperature. This modification was found essential because the high rate of strain hardening represented by a constant and temperature-independent n does not agree with experimental data for steels, including VAR 4340. It is interesting to note that in spite of relatively high level of hardness after the heat treatment (≈ 50 HRC) the VAR 4340 of high purity retained some plasticity in shear. This fact permits the analytical and numerical calculations discussed in the next part of this study.

The structure of the constitutive relation, Eq. (17), has some elements which are based on the material science approach. First of all, the stress level is normalized by $\mu(T)/\mu_0$ which takes into account the thermal softening of the crystalline lattice. The first expression in the brackets of Eq. (17) is simply the internal stress and the second is the strain rate and temperature-dependent effective stress (e.g. Klepaczko, 1987b).

The well-posedness of the problem has been assured by introduction of the rate-dependent constitutive relations (Lodygowski, 1995).

The number of constants in Eqs (17)–(19) amounts to 13; they are assembled in *table I*. To better illustrate the constitutive relation used in the numerical calculations, Eq. (17) is presented in graphic form in *figure 1* in 3-D as the yield stress in shear (plastic strain is zero) as a function of the absolute temperature and the logarithm of shear strain rate, *figure 1a;* in *figure 1b* a similar surface is presented for $\Gamma_p = 1.0$. The effect of temperature and strain rate on shear stress is more intense at lower temperatures and higher strain rates: this

is a typical behavior for steels. The solid line in *figure 1* shows the limit of the $f_4(\dot{\Gamma}, T)$ term in Eqs (16) and (17). For higher levels of plastic strain the general shape of the surface remains similar. A more exact analysis of the constitutive relation (17) is given elsewhere (Klósak and Klepaczko, 1996).

Table I. Material constants for VAR 4340 steel, $\approx$ 50 HRC.

Constant	Value (n = constant)	Value $n(T)$	Unit
B	1493.1	1493.1	MPa
μ_0	80769.0	80769.0	MPa
ν	0.1657	0.39	—
n	0.113	Eq. (19)	—
n_0	—	0.1354	—
m	2.7763	2.7763	—
T_0	300.0	300.0	K
Γ_0	1.6×10^{-3}	1.6×10^{-3}	—
$\dot{\Gamma}_0$	10^6	10^6	s^{-1}
A	5.047×10^{-4}	5.047×10^{-4}	K^{-1}
C	1.036×10^{-7}	1.036×10^{-7}	K^{-2}
D	2914.2	2914.2	K
τ_0	622.0	622.0	MPa

Since a large part of the plastic work is converted into heat, the temperature of the deformed material increases when the deformation time is relatively short. Without thermal conductivity the plastic deformation is purely adiabatic and the increase in temperature can be found by integration of Eq. (20), a relation analogous that of Eq. (5).

$$\left(\frac{dT}{d\Gamma}\right)_A = \frac{[1-\xi(\Gamma,T)]f_1(T)[f_2(T)f_3(\Gamma,T)+f_4(\Gamma,T)]}{J\rho_0(T)C_V(T)} \tag{20}$$

The stored energy in the lattice represented by $\xi(T,\Gamma)$ is usually a small fraction of the total plastic work (Bever et al., 1973) and the value of ξ does not exceed ≈ 0.1. Thus the coefficient of conversion $\beta = 1-\xi(T,\Gamma)$ is assumed constant, $\beta = 0.9$. Since $\rho(T)$ is only weakly dependent on temperature, it can be assumed as a constant. Although the exact expression for the specific heat $C_V(T)$ is temperature-dependent (e.g. Klepaczko and Rezaig, 1996), at temperatures > 300 K it may be also taken as a constant.

The balance of energy with heat conduction leads to the following 1–D relation

$$\beta\tau\frac{\partial\Gamma}{\partial t} = \rho C_v\frac{\partial T}{\partial t} - \lambda\frac{\partial^2 T}{\partial y^2} \tag{21}$$

where y is the direction of the heat conduction and λ is the heat conductivity (Fourier constant). All material constants associated with the thermal coupling are given in *table II*. The description of thermal coupling as outlined above permits numerical analyses to be made of all temperature-coupled problems as purely adiabatic as well as with the heat conduction. The total number of constants is 18 (i.e. 13 in *table I* and 5 in *table II*).

4. Numerical modeling by the FE method

The main target of the numerical analysis has been to explain differences between experimental results obtained with the direct impact on the MDS specimen (Klepaczko, 1994c) where CIV in shear was found, and the results of previous numerical calculations by the finite difference scheme where the initial conditions were not precisely specified (Klepaczko et al., 1988, 1993).

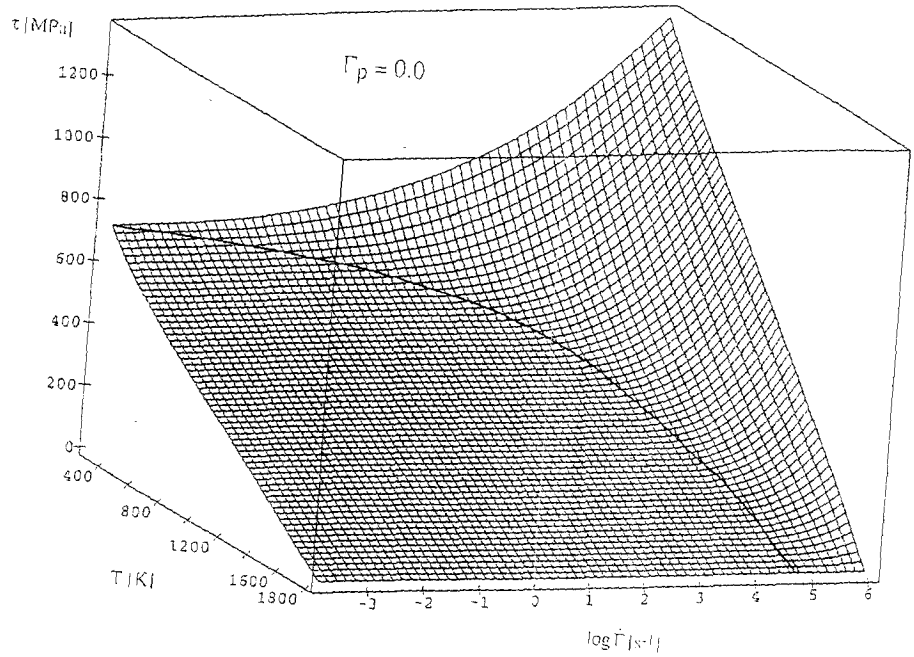

(a)

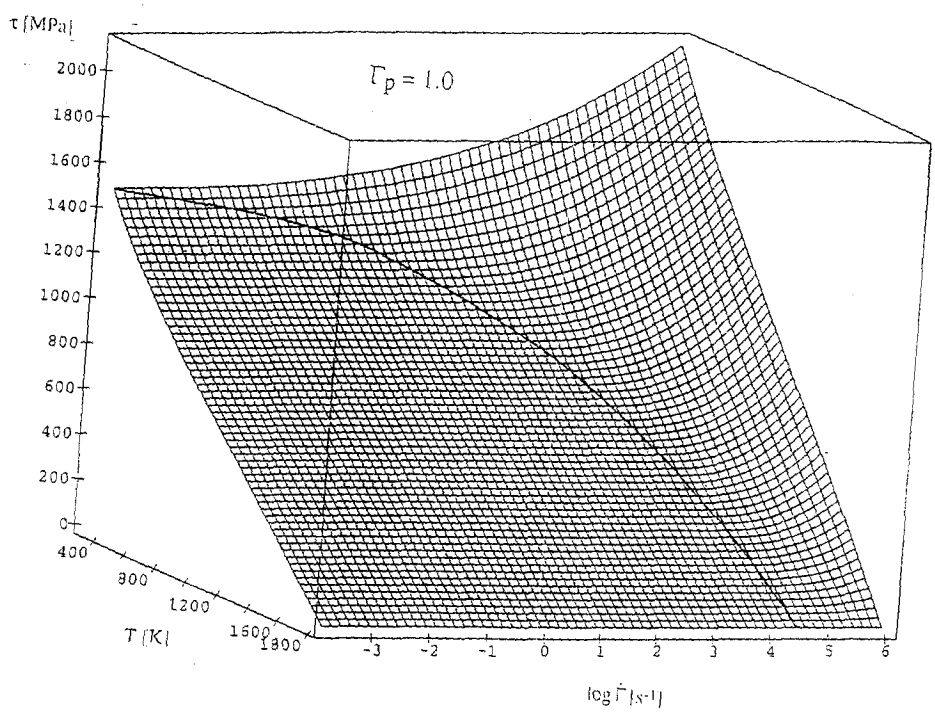

(b)

Figure 1. (a) Constitutive surface of the yield stress as a function of temperature and strain rate, $n = \text{const}$; (b) constitutive surface of the stress at $\Gamma_p = 1.0$ as a function of temperature and strain rate, $n = \text{const}$.

Table II. Material constants related to the thermal coupling VAR 4340 steel.

Constant	Value	Unit
β	0.9	—
λ	38.0	W mK^{-1}
ρ	7890	kg m^{-3}
C_v	460.0	J kg^{-1} K^{-1}
T_m	1812.0	K

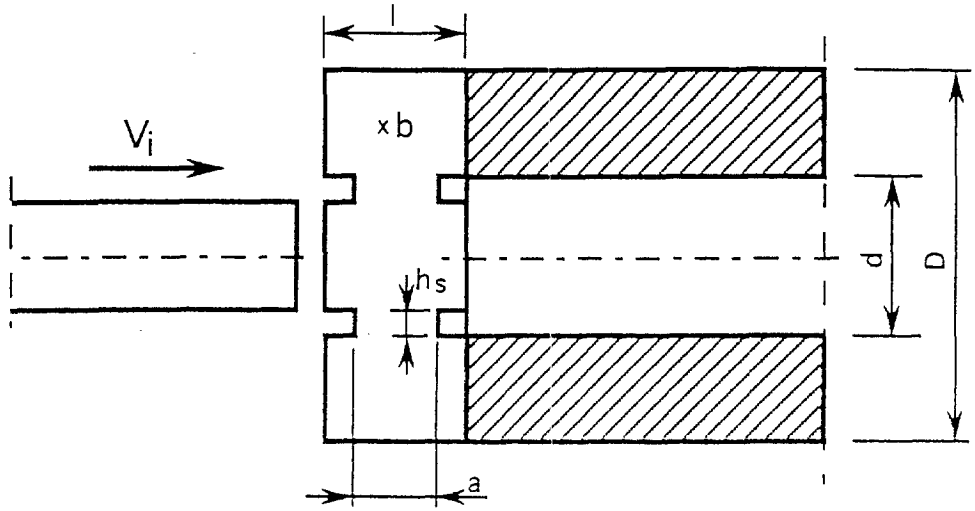

Figure 2. Scheme of the modified double shear specimen loaded by direct impact (Klepaczko, 1994c).

A general idea of the experimental technique based on the direct impact on the MDS specimen is shown in *figure 2*. The MDS specimen is loaded by the round projectile $\phi = 10\,\text{mm}$ with the impact velocity V_i, $1\,\text{m/s} \leq V_i \leq 200\,\text{m/s}$. The MDS specimen is supported by the Hopkinson tube where the transmitted elastic wave is measured. Displacement of the central part of the MDS specimen is measured as a function of time by an optical displacement transducer. There are two shearing zones in the specimen; the height of each is h_s, the length a and the thickness b. In real experiments $h_s = 2.0$ mm, $a = 5.0$ mm and $b = 6.0$ mm. The initial conditions are such that the imposed velocity on the shearing layers occurs at the surfaces closer to the projectile diameter. Since displacement of the Hopkinson tube is relatively small, the external shear layers practically do not move. This scheme of the experiment dictates the geometry of the numerical problem, as shown in *figure 3*. The height of the layer is assumed to be the same as in the MDS specimen, with $h_s = 2.0$ mm; the thickness changes along the y-axis according to the geometrical imperfection

$$b(y) = b_0\left[1 + \delta_w \sin\left(\frac{\pi}{2} - 2\pi\frac{y}{h}\right)\right] \tag{22}$$

where $\delta_w = 0.005$ is the geometric parameter which constitutes an imperfection of 1 %. Finally, the layer in the x-direction is assumed to be infinite, with $a \to \infty$. In general, it was intended to analyze CIV triggered by the shear banding phenomenon with the same simple geometry already assumed in previous numerical calculations (Klepaczko and Rezaig, 1996) and similar to MDS geometry. The difference between the numerical analysis and experiment lies in the fact that the numerics are limited to the infinite layer with the central imperfection, whereas in the MDS specimen the shear zone is finite.

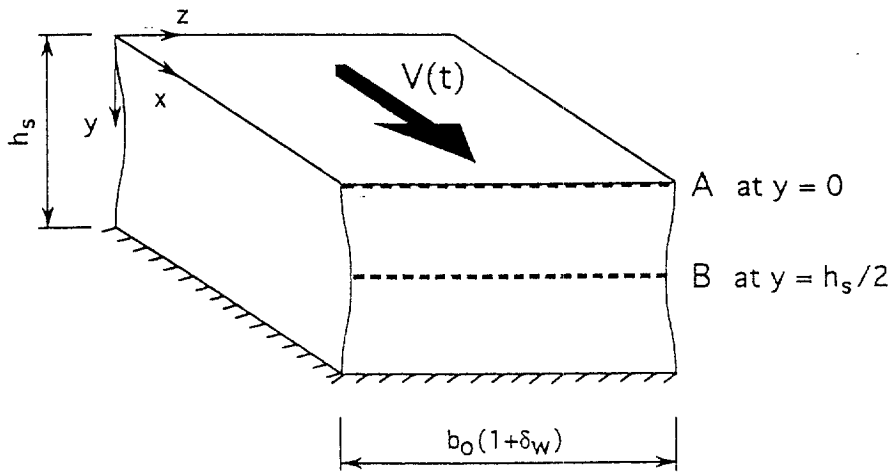

Figure 3. The infinite layer in the x-direction with geometry imperfection assumed in FE calculations.

In order to estimate the theoretical value of CIV for VAR 4340 steel at room temperature, an analysis by simple waves was performed as outlined in the previous section of the paper. The procedure was exactly the same, only the constitutive relation was changed, i.e. Eq. (17) with the material constants shown in *tables I* and *II*. Since the approach by simple waves is limited to only one adiabatic $\tau_A(\Gamma)$ curve, the strain rate assumed was $\dot{\Gamma} = 10^4\,\mathrm{s}^{-1}$. Integration of Eq. (12) can be divided into two steps

$$v_c = \int_0^{\Gamma_e} C_2 d\Gamma + \int_{\Gamma_e}^{\Gamma_m} C_{2p}(\Gamma) d\Gamma \tag{23}$$

and

$$v_c = C_2\Gamma_e + \int_{\Gamma_e}^{\Gamma_m} C_{2p}(\Gamma) d\Gamma \qquad \text{with} \quad C_2 = \left(\frac{\mu}{\rho}\right)^{1/2} \tag{24}$$

For high-quality steels including VAR 4340, the first term in Eqs (23) and (24) constitutes an important contribution to the v_c (CIV in shear). For such steels the rate of strain hardening $(\partial\tau/\partial\Gamma)_A$ is substantially reduced and the second term is not so high. If the strain hardening exponent n is assumed as a constant, then the nominal instability strain is $\Gamma_{nc} = 0.1695$ and the two terms in Eq. (24) are $v_{ce} = 51.1\,\mathrm{m/s}$ and $v_{cp} = 63.0\,\mathrm{m/s}$, CIV is $v_c = 114.1\,\mathrm{m/s}$. When n is temperature-dependent the instability strain is $\Gamma_{nc} = 0.1265$ and the two terms in Eq. (24) contribute to CIV as follows: $v_{ce} = 51.1\,\mathrm{m/s}$ and $v_{cp} = 57.0\,\mathrm{m/s}$; thus $v_c = 108.1\,\mathrm{m/s}$. These values are of the same order as those found in experiment for VAR 4340 steel, with CIV $\approx 130\,\mathrm{m/s}$, (Klepaczko, 1993).

Numerical analyses have been performed by the FE codes ABAQUS/Standard and ABAQUS/Explicit (ABAQUS Manual, 1995). A two-dimensional finite element model was applied. The plane strain behavior was assumed by using available 'plane strain' 2-D elements. In all calculations except $V_i = 2 \cdot 10^{-5}\,\mathrm{m/s}$, CPE4R elements were used. For $V_i = 2 \cdot 10^{-5}\,\mathrm{m/s}$ the element CPE4T was applied. Taking into account the fact that there were two expected shearing modes three kinds of meshing were used: the first was for shearing in the mid-layer (*figure 4a*); the second for transitional shearing (*figure 4b*), i.e. simultaneously in the middle and in the top layer; and finally, the mesh for plastic shearing trapped near the upper surface (*figure 4c*). In general, the mesh of 60 × 19 elements was used with density respecting the experimentally measured thickness of the shear band, (Klepaczko, 1994c). Three other mesh densities were also proposed to study mesh dependence (*figure 17*).

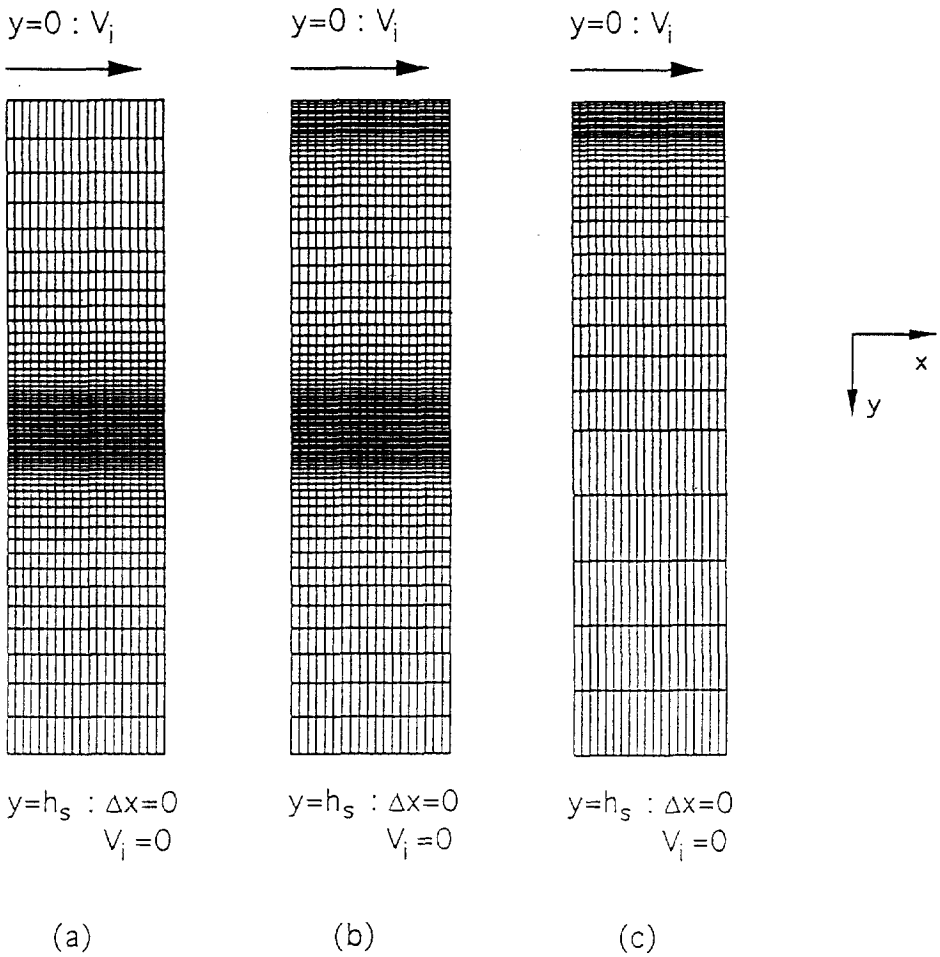

Figure 4. Three meshes used in FE calculations at increasing impact velocities V_i.

In order to model the direct impact more closely, the initial conditions in velocity at $y = 0$ were assumed in the form of the finite rise time. A schematic representation of the rise time function is shown in *figure 5*. The velocity at $y = 0$ increases from zero to the final level during the short and finite interval of time. The total rise time t_m is chosen according to the Gaussian cumulative distribution function. The value of t_m is chosen according to the final velocity level, V_i. The main reason for using this function is that it possesses an acceleration and deceleration consistent with a physical intuition. The mathematical form of the rise time function is given by Eq. (25).

$$F(x) = \int_{x_{\min}}^{x} \frac{1}{\sqrt{2\pi\sigma^2}} \exp\left(-\frac{(X-m)^2}{2\sigma^2}\right) dX \tag{25}$$

Values of the rise time were assumed as follows: $t_m = 10^{-2}$ s for $V_i < 1$ m/s, $t_m = 10^{-6}$ s for $1 \text{ m/s} < V_i \leq 20$ m/s and $t_m = 10^{-7}$ s for $V_i \geq 20$ m/s. Values of parameters m and σ in Eq. (25) were $m = 0.5$ and $\sigma = 0.125$.

Depending on the imposed velocity at $y = 0$, the problem was considered either by heat conduction or by an adiabatic approach. The latter case leads to the modification of Eq. (21) due to disappearance of the last term ($\lambda = 0$). The ABAQUS code provides both types of analysis; however, certain restrictions are imposed. Thus,

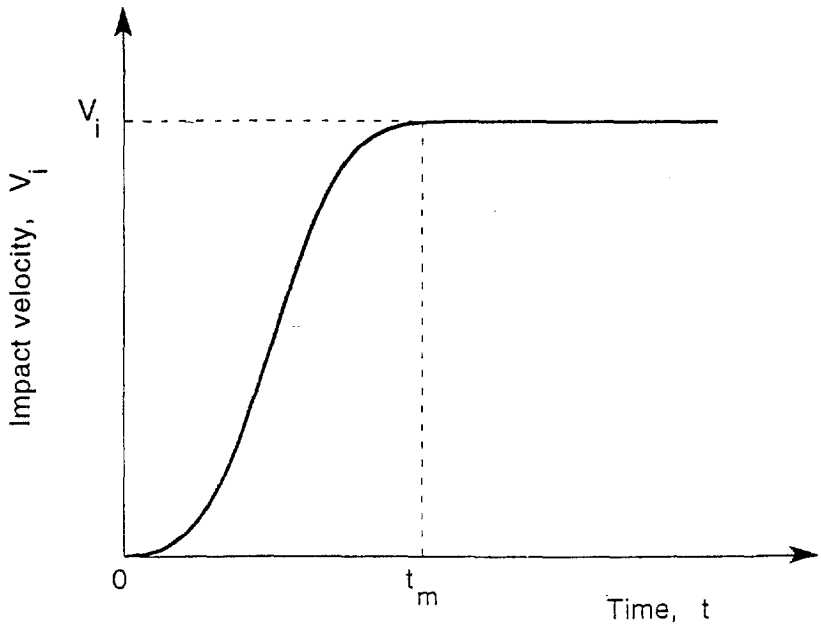

Figure 5. Schematic representation of the rise time function, Eq. (25).

in the analysis with heat conduction (fully coupled temperature-displacement problem) the inertia effects are neglected; on the other hand, the analysis with the wave effects is assumed to be adiabatic.

Table III gives an overview of the performed tasks. The velocity V_i was increased from $V_i = 2 \cdot 10^{-5}$ m/s to 160 m/s in 17 steps. All calculations in this series were performed for the temperature-dependent exponent, $n(T)$. In the case of the quasi-static loading treated with heat conduction, first-degree thermal conditions were imposed at the bottom and top surfaces, i.e. a constant temperature of 300 K was assumed.

Table III. Performed tasks in FE analysis with calculated nominal instability strain Γ_{nc} and localization strain Γ_{nl}.

No.	Impact velocity V_i [m s^{-1}]	Nominal strain rate $\dot{\Gamma}_n$ [s^{-1}]	Instability strain Γ_{nc}	Localization strain Γ_{nl}
V_1	2×10^{-5}	10^{-2}	∞	∞
V_2	0.2	10^2	0.346	0.405
V_3	2.0	10^3	0.290	0.576
V_4	20.0	10^4	0.165	0.580
V_5	40.0	2×10^4	0.180	0.540
V_6	60.0	3×10^4	0.185	0.560
V_7	80.0	4×10^4	0.210	0.630
V_8	90.0	4.5×10^4	0.220	0.640
V_9	100.0	5×10^4	0.220	0.660
V_{10}	105.0	5.25×10^4	0.210	0.470
V_{11}	110.0	5.5×10^4	0.200	0.350
V_{12}	115.0	5.75×10^4	0.180	0.270
V_{13}	120.0	6×10^4	0.008	0.159
V_{14}	125.0	6.25×10^4	0.007	0.120
V_{15}	130.0	6.5×10^4	0.006	0.020
V_{16}	140.0	7×10^4	0.002	0.008
V_{17}	160.0	8×10^4	0.002	0.007

5. Results of FE calculations

The effect of the temperature dependence on the strain-hardening exponent n [Eq. (19)] was first examined. The results in the form of adiabatic $\tau_A(\Gamma)$ curves for $V_i = 20$ m/s are shown in *figure 6*. If n is temperature-dependent, the instability point (τ_m, Γ_{nc}) where τ_m is the maximum shear stress and Γ_{nc} is the nominal shear strain at τ_m is shifted into smaller strains in comparison to the result with $n = \text{const}$: $\Gamma_{nc} = 0.235$ and $\Gamma_{nc} = 0.174$, respectively. There is a big difference between the values of the final localization strains Γ_{nl}. The final localization strain was defined in all FE calculations by the minimum tangent modulus $\partial\tau/\partial\Gamma_n = -7 \cdot 10^3$ MPa. The nominal shear strain Γ_n is defined by the mean displacement gradient at $y = 0$, $\Gamma_n = \Delta x/h_s$ (*figure 3*), with $h_s = 2.0$ mm. If n depends on temperature, the localization strain substantially decreases. It indicates the importance of the temperature dependence on the rate of strain hardening in steels. *Figure 3* also defines the positions of the analyzed cross-sections called A and B. The cross-section A is located at the top ($y = 0$), where the impact velocity V_i is imposed. The cross-section B is located in the middle of the layer, where the geometrical defect produces the smallest cross-section area. The symbols in the figures which follow are explained below: i) plastic shear strain Γ_A is the current shear strain determined at the cross-section A; ii) plastic shear strain Γ_B is the current shear strain determined at the cross-section B; iii) critical nominal shear strain Γ_{nc} is the strain corresponding to the condition $\partial\tau_A/\partial\Gamma = 0$ (maximum stress) and can be estimated from the curves $\tau(\Gamma_n)$; iv) τ_A is the shear stress at $y = 0$, determined in experiments with MDS geometry.

At lower impact velocities, due to geometric imperfection the localization occurs in the middle of the layer, that is in the cross-section B, whereas at impact velocities > 103 m/s, localization occurs near cross-section A. This is demonstrated in *figure 7* where the displacement fields are shown for two impact velocities, $V_i = 40$ and $V_i = 130$ m/s. A *complete* change in the displacement field from the 'quasi-static' to a pure 'dynamic' mode should be noted. This transition is caused by CIV in the shear. The difference in the shear strain evolution in

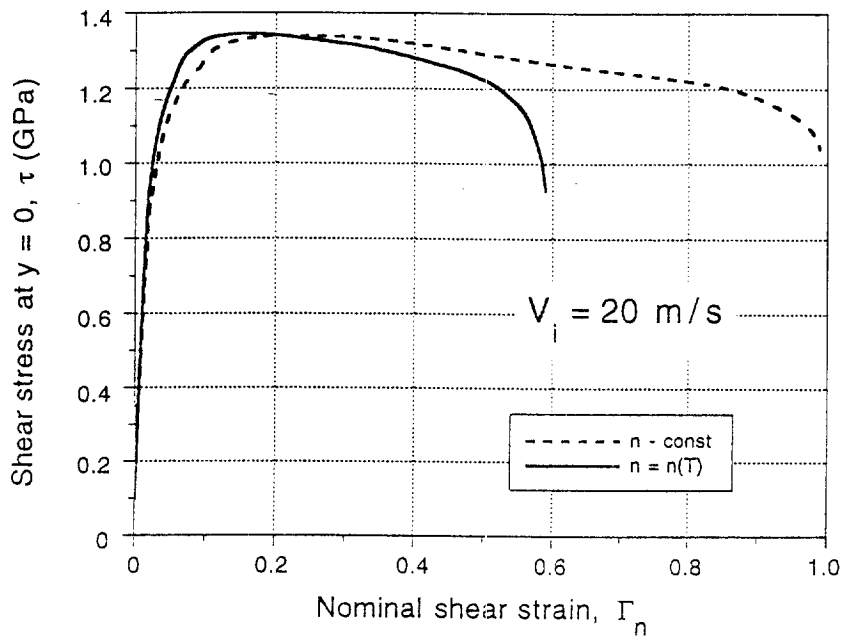

Figure 6. Reconstituted adiabatic $\tau_A(\Gamma)$ curves for two cases of the strain hardening exponent n and $n(T)$ as defined by Eq. (19); VAR 4340 steel, $\simeq$ 50 HRC.

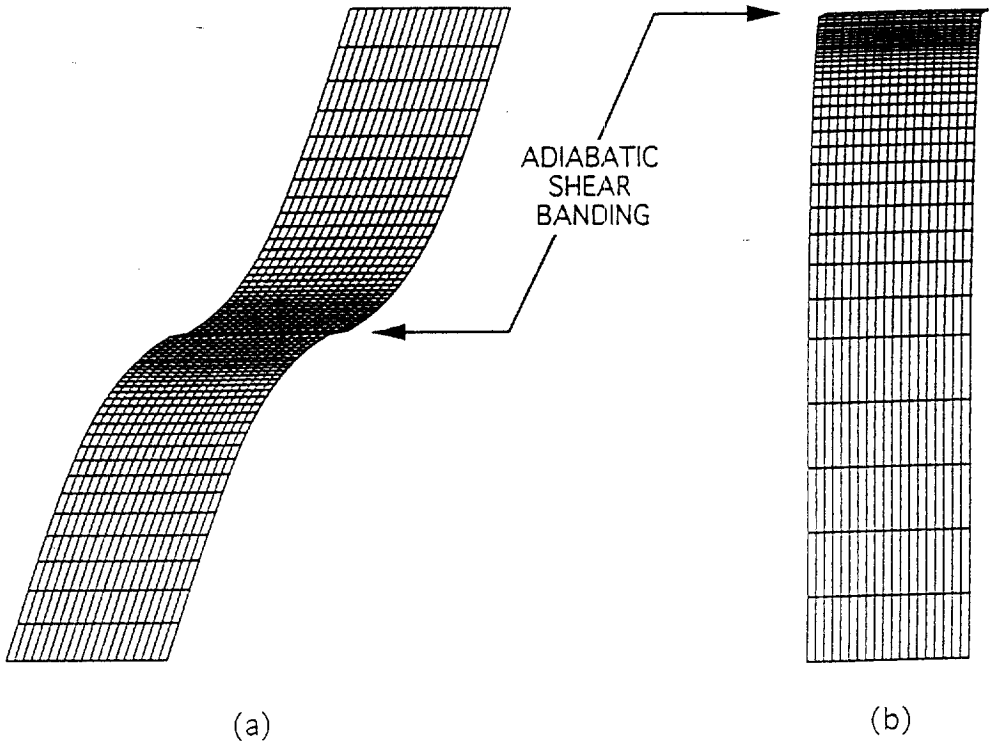

Figure 7. Two displacement fields for two different impact velocities, (a) $V_i = 40$ m/s; (b) $V_i = 130$ m/s.

cross-sections A and B as a function of the nominal strain Γ_n, i.e. the Marciniak plots, are shown respectively for $V_i = 40$ and $V_i = 115$ m/s in *figures 8* and *9*. Although the nominal strain rate in *figure 8* is $\dot{\Gamma}_n = 2 \cdot 10^4$ s^{-1}, the evolution of Γ_A and Γ_B is typical for a layer with an imperfection deformed quasi-statically.

On the contrary, the Marciniak plot shown in *figure 9* for $V_i = 115$ m/s, $\dot{\Gamma}_n = 5.75 \cdot 10^4$ s^{-1} is completely inversed; the bulk of plastic deformation and localization occurs in the cross-section A, and the evolution of plastic deformation in the cross-section B is substantially reduced. This indicates that the impact velocity 115 m/s is very close to CIV in shear. Comparison of spatial distributions of the local strain rate at four impact velocities at the assumed end of localization, $\partial\tau/\partial\Gamma_n = -7 \cdot 10^3$ MPa, is shown in *figure 10*. At an impact velocity $V_i = 130$ m/s, practically all plastic deformation is localized at $y = 0$, indicating the wave trapping of plastic shearing. A similar tendency is observed with spatial distributions of temperature for the same set of impact velocities (*figure 11*). It is clear that the maximum increase in temperature in the middle of the shearing zone may be quite high (around 1000 K in the cross-section B for $V_i = 100$ m/s). At higher impact velocities above CIV, the local temperatures at the cross-section A may be even higher reaching values close to the melting point. This was confirmed by SEM for VAR 4340 steel (Klepaczko, 1993). The local strain rates in the cross-section A are also very high, for example for the impact velocity $V_i = 130$ m/s, $\dot{\Gamma} \approx 2 \cdot 10^6$ s^{-1} (*figure 10*). It is interesting to note that at high impact velocities but lower than CIV, the maxima of strain rate and temperature are shifted off-center. This is caused by the plastic wave propagation in the layer interior. Another observation is a slight increase in critical nominal shear strains Γ_{nc} beginning from ≈ 40 m/s. This is caused in turn by the competition between two extreme deformation fields shown in *figure 7*. Such behavior is also clear from *figure 10*.

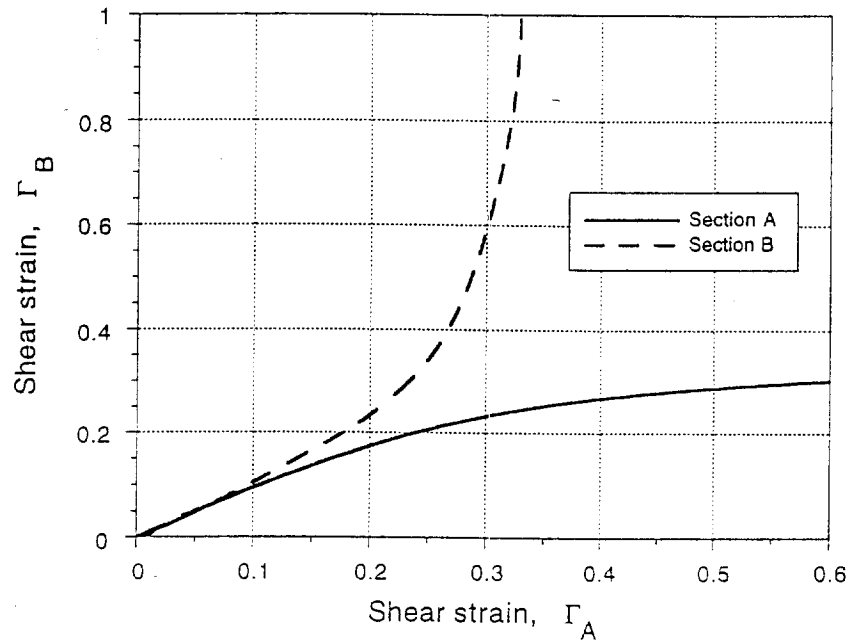

Figure 8. Marciniak plot showing evolution of shear strain in cross-sections A and B at $V_i = 40$ m/s, $\dot{\Gamma}_n = 2 \cdot 10^4\,\mathrm{s}^{-1}$.

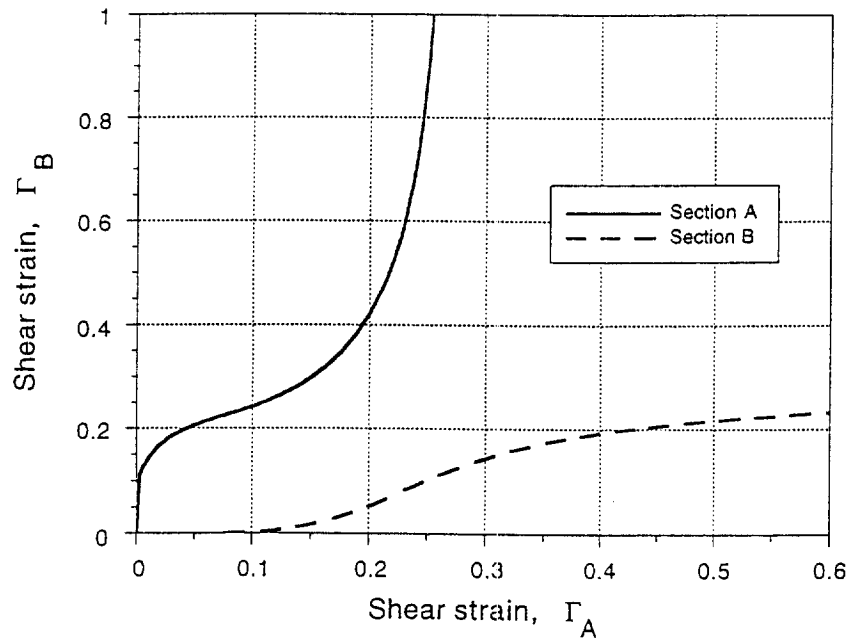

Figure 9. Marciniak plot showing evolution of shear strain in cross-sections A and B at $V_i = 115$ m/s, $\dot{\Gamma}_n = 5.75 \cdot 10^4\,\mathrm{s}^{-1}$.

The most important observation is that the $\tau_A(\Gamma_n)$ curves differ substantially at different impact velocities. This is demonstrated in *figures 12* and *13*. In the range of lower impact velocities, the $\tau_A(\Gamma_n)$ curves reflect a real behavior of material; this is true up to $V_i \approx 40$ m/s, $\dot{\Gamma} \approx 2 \cdot 10^4\,\mathrm{s}^{-1}$. The $\tau_A(\Gamma_n)$ curve determined at this velocity shows a characteristic stress peak at very small strains. In addition, the initial slope in the 'elastic' range

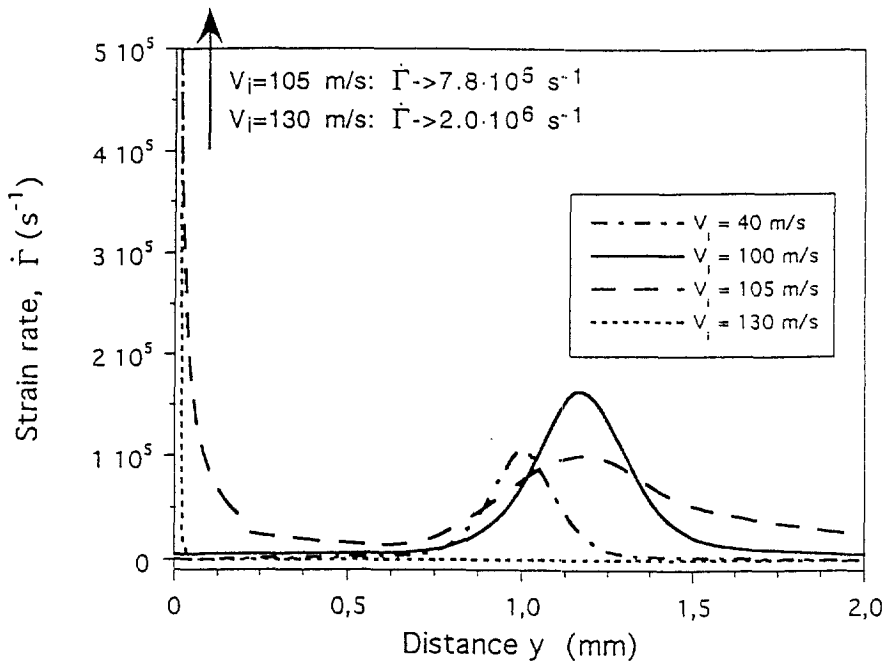

Figure 10. Spatial distributions of shear strain rate for four impact velocities at the end of localization, $(\partial\tau/\partial\Gamma_u) = -7 \cdot 10^3$ MPa.

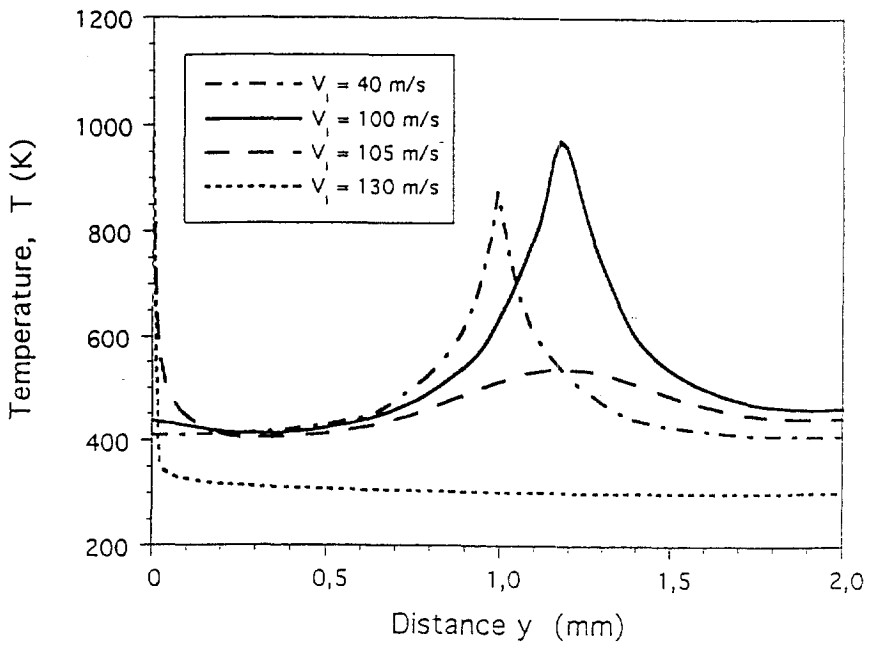

Figure 11. Spatial distributions of temperature for four impact velocities at the end of localization, $(\partial\tau/\partial\Gamma_u) = -7 \cdot 10^3$ MPa.

becomes much steeper than predicted by the shear modulus. This results from the interaction of plastic waves and adiabatic instability near the cross-section A. When the impact velocities are still higher, the maximum of shear stress occurs at very small nominal strains (*figure 13*).

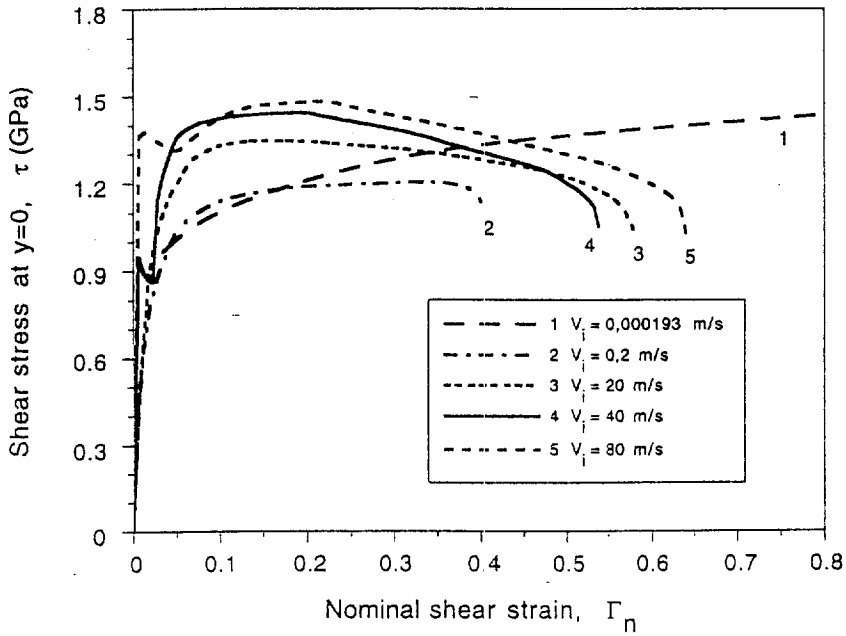

Figure 12. Shear stress versus nominal strain determined from displacement of cross-section A; impact velocities lower than CIV.

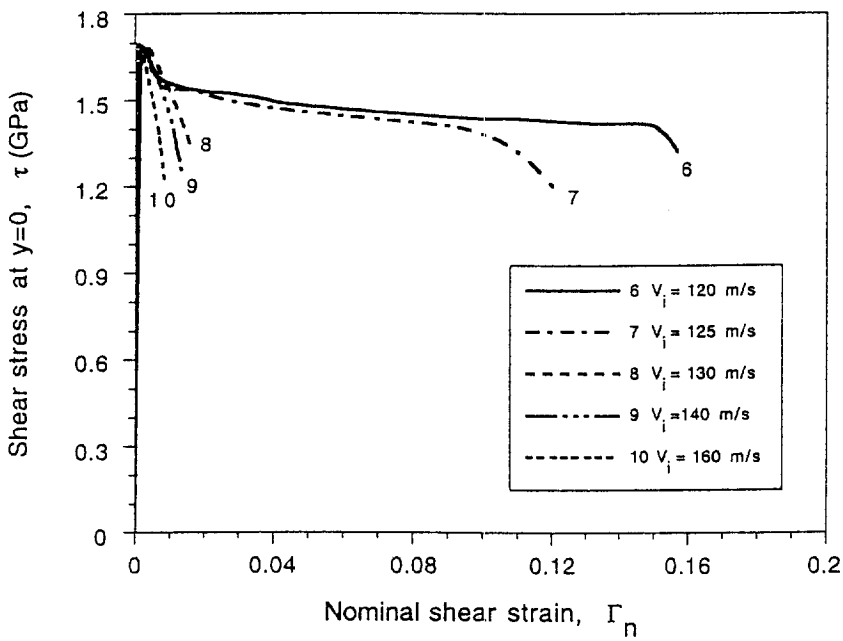

Figure 13. Shear stress versus nominal strain determined from displacement of cross-section A; impact velocities close to and above CIV.

The slopes $(\partial\tau/\partial\Gamma)_A$ after the stress maxima are negative and decrease very rapidly when the impact velocities are high enough. This indicates that the CIV is reached. The instability points appear almost instantaneously with a still shorter process of localization. In *figure 14* are shown, normalized by μ (the shear modulus), the

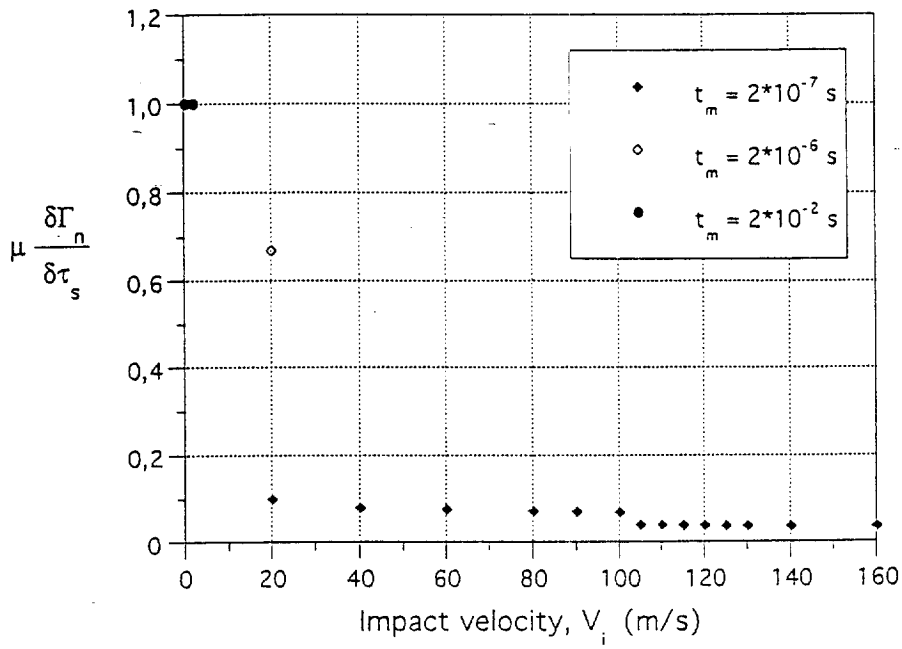

Figure 14. Nominal slopes of $\tau_A(\Gamma)$ curves.

initial slopes of the $\tau_A(\Gamma_n)$ curves as a function of impact velocity V_i. At low velocities the slopes are equal to μ, but at higher loading rates they are much steeper. The normalized slopes also depend on the rise time.

The sequence of previous figures clearly demonstrates a substantial evolution in shear stress $\tau_A(\Gamma_n)$ determined at $y = 0$ when the impact velocity is increased. Such curves can be determined from the MDS tests.

It is clear that the CIV phenomenon is a *process* in which the transition is not instantaneous. Consequently, the analytical solutions for CIV, as presented in the first part of this paper, can provide an approximate value of CIV in shear. The analytical value of CIV obtained for VAR 4340 steel, that is ≈ 110 m/s, is almost of the same order as that calculated by the FE method. CIV estimated for this steel from the FE simulations is ≈ 103 m/s, i.e. the beginning of the CIV transition zone.

Figure 15 shows the effect of mesh density on the global response of the model. It clearly demonstrates the proper posedness of the problem, but also highlights the secondary mesh dependence in localization zone. The 60×19 discretization can be considered as the lower limit, and a more refined meshing would be appropriate.

Finally, the complete series of calculations has been focused on the analysis of the instability point as determined by $\partial\tau_A/\partial\Gamma = 0$ and the localization process up to $(\partial\tau_A/\partial\Gamma_n)_{\min}$. The main parameter in these calculations was the imposed velocity V_i. All values of V_i along with the values of the nominal strain rates and obtained values of Γ_{nc} and Γ_{nl} are presented in *table III*. The main conclusion drawn from *table III* is that under the isothermal conditions of deformation ($V_i = 2 \cdot 10^{-5}$ m/s) in the absence of thermal softening, the instability strain is infinite. When the impact velocity is increased beginning from $V_i = 0.2$ m/s, the instability strain is finite, i.e. $\Gamma_{nc} = 0.346$. Thus an increase in the imposed velocity V_i leads to a decrease in the critical strains. All values of Γ_{nc} and Γ_{nl} in *table III* are also shown in *figure 16* as a function of the impact velocity V_i. The sequence of points indicates a complicated interplay between thermal coupling and wave processes. Three regions can be recognized; in the first the ratio of the localization strain Γ_{nl} to the instability strain Γ_{nc} is almost constant. The second region from $V_i = 103$ to $V_i = 130$ m/s is characterized by the beginning of thermoplastic

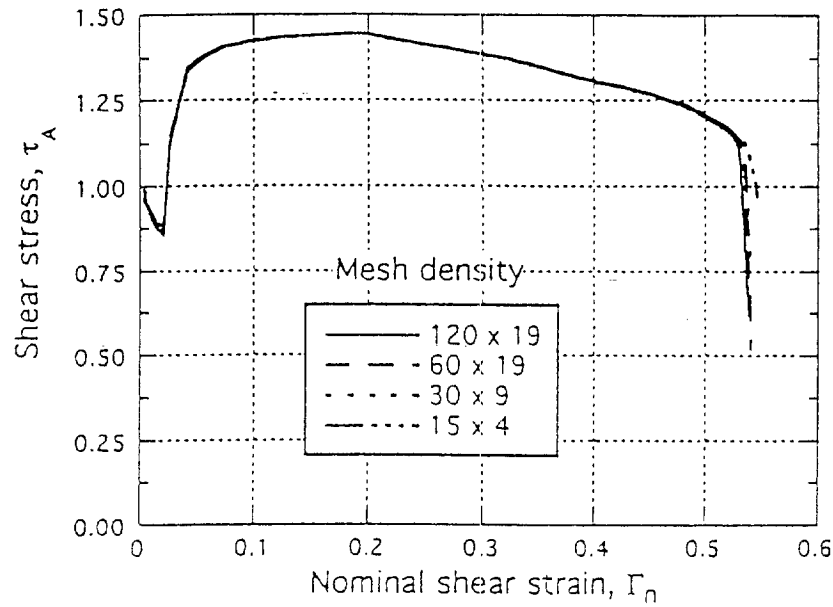

Figure 15. Effect of mesh density, $V_i = 40$ m/s; shear stress at the cross-section A versus nominal shear strain.

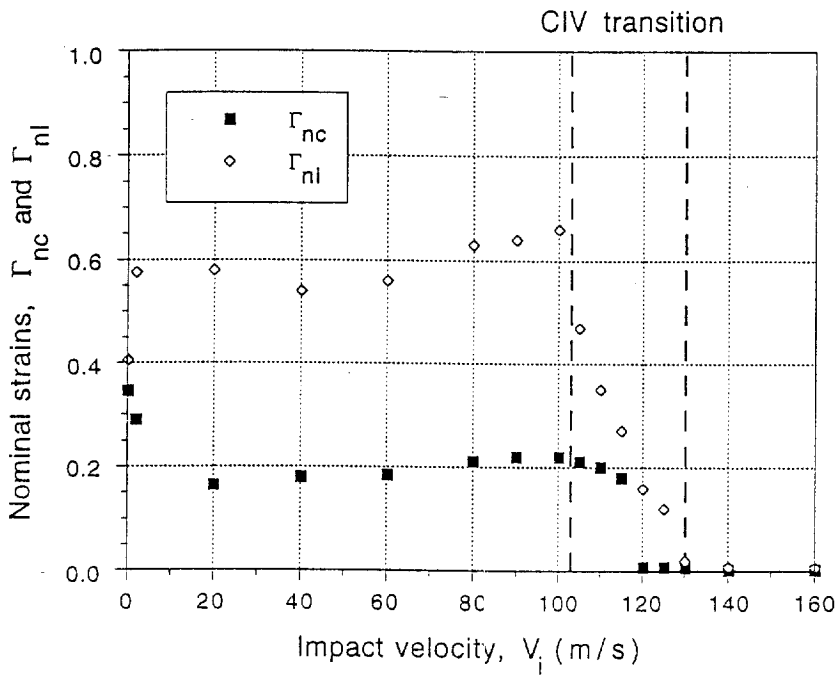

Figure 16. Nominal shear strains of instability Γ_{nc} and localization Γ_{nl} as a function of impact velocity V_i.

deformation trapping by plastic waves. The most substantial change in the instability strain Γ_{nc} occurs between velocities $V_i = 115$ and $V_i = 120$ m/s, and the values of Γ_{nc} are respectively $\Gamma_{nc} = 0.18$ and $\Gamma_{nc} = 0.008$. A similar transition occurs with the localization strain Γ_{nl} at slightly higher values of V_i, i.e. between 125 and

130 m/s. Finally, in the third region at impact velocities > 130 m/s the trapping is complete and instantaneous instability and localization occurs with a very small localization strain, typically Γ_{nl} in the order of $\simeq 0.002$.

CIV in shear has far-reaching consequences on fragmentation. Experiments performed with MDS specimens consisting of VAR 4340 steel (Klepaczko, 1993) clearly indicated a decrease in the fracturing energy when the impact velocity exceeded $\simeq$ 130 m/s. In order to estimate the fracture energy by the FE method as a function of the impact velocity, the $\tau_A(\Gamma_n)$ curves have been integrated up to the localization strain Γ_{nl}. The results for all 17 simulations are shown in *figure 17*. Within the first region the fracture energy increases up to $E = 681\,\mathrm{MJ/m^3}$ for $V_i = 100$ m/s and next, in the second region, a considerable decrease occurs; for impact velocity $V_i = 130$ m/s the energy reaches a level of $\simeq 8\,\mathrm{MJ/m^3}$. In the third region the fracture energy stays almost constant on a level from 6 to $8\,\mathrm{MJ/m^3}$. Thus, the energy drop is practically 100-fold. Different scales should be used to show the energy level for velocities > 130 m/s.

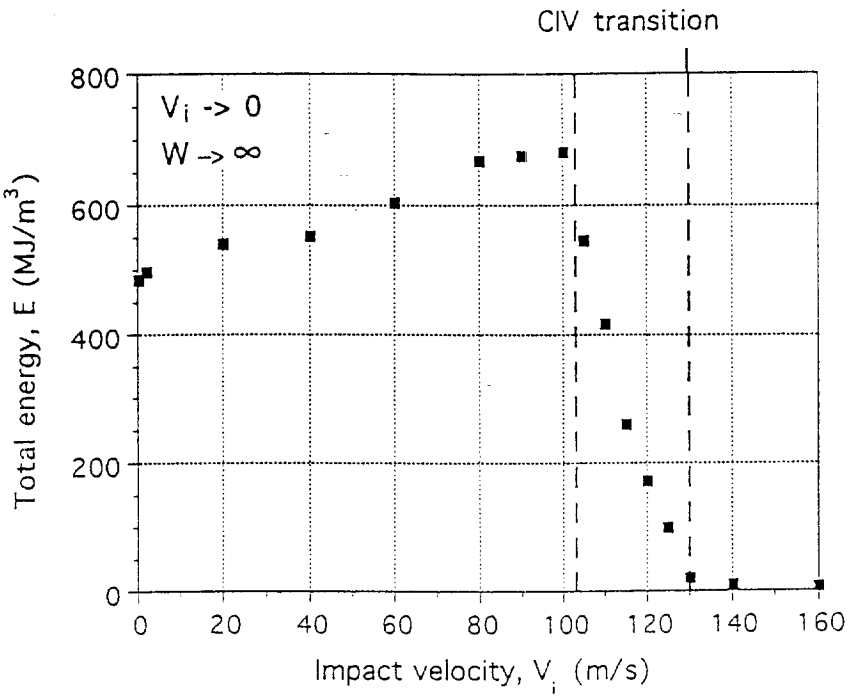

Figure 17. Fracture energy versus impact velocity V_i.

6. Discussion and conclusions

The infinite layer of the height $h_s = 2.0$ mm with a small geometrical imperfection, loaded by impact shear from one side and assumed to be stationary on the other side was taken into consideration. As an example, the behavior of VAR 4340 steel at $\approx$ 50 HRC was analyzed. The study of plastic instability by wave trapping and adiabatic heating has revealed several new features. The most important observation is the transition of the displacement and deformation fields. At lower impact velocities up to 40 m/s the fields are identical, as under quasi-static conditions. When the impact velocity exceeds 40 m/s, the deformation fields are distorted by plastic waves and both mechanisms of deformation compete, i.e., the quasi-static mode and a new mode of deformation caused by plastic waves. When the impact velocity exceeds 103 m/s, the mode caused by plastic waves starts to

dominate and the CIV in shear occurs. If the impact velocity exceeds 130 m/s, complete deformation trapping occurs near the impact end of the layer due to thermoplastic instability caused by plastic waves.

The FE analyses have revealed the phenomenon of CIV in shear and shown that the whole transition into complete deformation trapping that occurs within certain range of impact velocities, in the present case $103\ \mathrm{m/s} \leq V_i \leq 130\ \mathrm{m/s}$. The analytical methods discussed in the first part of this paper may only be used as a first approximation in finding the CIV in shear.

It has been confirmed that the experimental technique with the MDS specimen loaded by direct impact is a reliable tool for finding stress–strain relations at high strain rates up to $\sim 5 \cdot 10^4\ \mathrm{s}^{-1}$. This technique may also serve in the determination of the CIV in shear. In spite of some differences in geometries studied by FE and those applied in experiments, a very good agreement has been found between experimental and FE values of the CIV in shear for VAR 4340 steel. More detailed analyses of the shearing zones have shown substantial local increases in temperature and strain rate. The temperature increase in the ASB core may reach 700 K. The local strain rate may be also very high. For example, at an impact velocity of $V_i = 130\ \mathrm{m/s}$ where an intense wave trapping occurs, the local strain rate is in the order of $2 \cdot 10^6\ \mathrm{s}^{-1}$.

Finally, the effect of CIV in shear must be taken into account in fragmentation processes developed by impact or explosions (e.g. Erlich et al., 1980). When the local velocity of sliding exceeds the CIV in shear for a particular material, the energy of fragmentation or perforation diminishes rapidly by interaction between the ASB and the CIV in shear. For the VAR 4340 steel at ~ 50 HRC, the drop in energy expended to reach the final localization stage before and after CIV is $\sim$ 100-fold.

In conclusion, it has been demonstrated in this study that on the one hand, the CIV in shear is an important process in ASB, and on the other that the FE technique is sufficiently advanced to find more details on the mechanisms of fast plastic deformation coupled with temperature and plastic waves. It should be noted, however, that special care is required in FE techniques where advanced stages of localization with temperature coupling are expected. In such cases, because of high temperature gradients, the adiabatic scheme can no longer be used.

Acknowledgements

The research reported herein was sponsored in part by the US Army through its European Research Office, Contract DAJA M68171-95-C-9071, and in part by the CNRS–France.

References

ABAQUS Manual, Version 5.5, Hibbit, Karlsson and Sorensen Inc; Providence, RI, USA, 1995.

Bai Y., Dodd B., Adiabatic Shear Localization, Pergamon Press, 1992.

Bever M.B., Holt D.L., Titchener A.L., 1973, The stored energy of cold work, Progress in Materials Science, Pergamon Press, Oxford, vol. 17, 1973.

Cowie J.G., The influence of second-phase dispersions on shear instability and fracture toughness of ultrahigh strength 4340 steel, US Army Mat. Tech. Lab. Rep. (1989) MTL-TR 89-20.

Dormevel R., The adiabatic shear phenomemon, in: Mater. High Strain Rates, Elsevier Appl. Sci., London, 1987, p. 47.

Erlich D.C., Curran D.R., Seaman L., Further development of a computational shear band model. SRI Int. Rep., (1980) AMMRC TR80-3.

Kàrmàn T., Duvez P.E., The propagation of plastic deformation in solids, J. Appl. Phys., 21 (1950) 987.

Klepaczko J.R., Generalized conditions for stability in tension tests, Int. J. Mech. Sci., 10 (1968) 297.

Klepaczko J.R., A practical stress–strain–strain rate–temperature constitutive relation of the power form, J. Mech. Working Technol., 15 (1987a) 143.

Klepaczko J.R., Modeling of structural evolution at medium and high strain rates, FCC and BCC structures, Constitutive Relations and Their Physical Basis, Proc. 8th Risö Mater. Symp., p. 387, Risö, Denmark, 1987b, p. 387.

Klepaczko J.R., Lipinski P., Molinari A., An analysis of the thermoplastic catastrophic shear in some metals, in: Impact Loading and Dynamic Behaviour of Materials, DGM Informationsgesellschaft Verlag, Oberursel, vol. 2, 1988, p. 695.

Klepaczko J.R., Experimental investigation of adiabatic shear banding at different impact velocities, Final Tech. Rep. US Army Eur. Res. Office, DAJA 49-90-C-0052, LPMM, Metz Univ., France, 1993.

Klepaczko J.R., Plastic shearing at high and very high strain rates: Proc. Conf. Eurodymat, J. Phys. IV4 (1994a) C8-35.

Klepaczko J.R., Some results and new experimental technique in studies of adiabatic shear bands, Arch. Mech., 46 (1994b) 201.

Klepaczko J.R., An experimental technique for shear testing at high and very high strain rates; the case of mild steel, Int. J. Impact Eng., 15 (1994c) 25.

Klepaczko J.R., On the critical impact velocity in plastic shearing: Explomet'95, Proc. Int. Conf. Metallurg. Mater. Appl. Shock-Wave and High-Strain-Rate Phenomena, Elsevier Sci. Publ., Amsterdam, 1995, p. 413.

Klepaczko J.R., Rezaig B., A numerical study of adiabatic shear banding in mild steel by dislocation mechanics based constitutive relations, Mech. Mater., 18 (1996) 125.

Klósak M., Klepaczko J.R., Numerical study of the critical impact velocity in shear. Appendix 1, Final Tech. Rep. US Army Eur. Res. Office, DAJA N68171-95-C-9071, LPMM, Metz University, France, 1996.

Lodygowski T., On avoiding of spurious mesh sensitivity in numerical analysis of plastic strain localization. Comp. Ass. Mech. Eng. Sci., 2 (1995) 231.

Meyer L.W., Staskewitsch E., Mechanical behaviour of some steels under dynamic loading, Impact Loading and Dynamic Behaviour of Materials, DGM Informationsgesellschaft Verlag, Oberursel, vol. 1, 1988, p. 331.

Recht R.F., Catastrophic thermoplastic shear, J. Appl. Mech., 86 (1964) 189.

Rogers H.C., Adiabatic Shearing–An Overview, Drexed Univ. Rep., 1974.

Tanimura S., Duffy J., Strain rate effects and temperature history effects for three different tempers of 4340 VAR steel, ARO, USA, Rep. No-DAAG 29-81-K-0121/4 (1984).

Wu F.H., Freund L.B., Deformation trapping due to thermoplastic instability in one-dimensional wave propagation, J. Mech. Phys. Solids, 32 (1984) 119.